Journal of Applied Sciences

ISSN 1812-5654

science alert

ANSInet
an open access publisher
http://ansinet.com

Journal of Applied Sciences 11 (22): 3663-3676, 2011
ISSN 1812-5654 / DOI: 10.3923/jas.2011.3663.3676

Modelling and Control of a Residential Wind/PV/Battery Hybrid Power System with Performance Analysis

[1]A. Yasin, [2]G. Napoli, [2]M. Ferraro and [2]V. Antonucci
[1]Scuola Superiore di Catania, Via Valdisavoia 9, Catania, Italy
[2]CNR-ITAE, Consiglio Nazionale delle Ricerche, Instituto di Tecnologie Avanzate per l'Energia, "Nicola Giordano" Via Salita S. Lucia Sopra Contesse 5-98126 Messina, Italy

Abstract: Time domain performance analysis results of a standalone hybrid system are presented based on commercial wind generator, photovoltaic generator and battery energy storage system. The hybrid system is designed and modelled using Matlab/Simulink/SimPowSys™ environment, a control strategy has been proposed to control the voltage DC bus and the energy flow between the different energy sources. The wind and photovoltaic generators are controlled locally to obtain the maximum power extraction, while battery energy storage system is controlled using specific control strategy depending on the voltage of the DC bus and energy flow. To test the performance of the system three different cases were analyzed; one case is the examination of the system performance when the photovoltaic generator is excluded from the system, the second case excludes wind energy generator while the third case includes all the sources. Each case contains various operating conditions and disturbances of load and weather data. The frequency deviation, stability of DC bus voltage and voltage total harmonic distribution are taken as system performance indexes. The simulation results ensure the effectiveness of the proposed hybrid system control strategy in following up the variations in load demand and weather data, providing the ground for practical realization.

Key words: Hybrid system, wind energy, photovoltaic energy, battery energy storage system, time domain performance analysis

INTRODUCTION

The accelerating concerns over global warming and the shortage of conventional energy sources have led to increased interest in distribution Generation Sources (DG) based on green energies. Wind and photovoltaic energy are the most examined and developed renewable energy sources all over the world. Photovoltaic Energy Conversion System (PVECS) is becoming one of the most important renewable energy resources, since it is clean, generated on-site, pollution free and inexhaustible (Grandi *et al*., 2003; Kuo *et al*., 2001). The high initial cost, low generation efficiency and lack of reliability are the major disadvantages of PVECS (Shimizu *et al*., 2007).

Wind Energy Conversion Source (WECS) is a sustainable future energy source which contributes to clean air and global safety, it's costs decrease with time in which the traditional fuels costs increase with time (El-Khattam and Salama, 2004). The generation of electricity utilized from wind is feasible for isolated places far away from the grid. The annual growth rate of wind energy utilization is 30% which is the fastest growth in the world (Ackermann, 2005).

Battery Energy Storage System (BESS) is of a great importance in enhancing hybrid systems, stabilizes and permits the system to run at a constant and stable output despite load fluctuations and it covers the deficiency in energy through instantaneous lacks of primary energy in case of sun and wind sources. Battery technologies have been improved significantly in order to meet the challenges of utility applications (Ribeiro *et al*., 2001). The high energy density, high energy capability, round trip efficiency, cycling capability, life span and initial cost are key factors of batteries for storage applications (McDowall, 2000).

Different types of battery technologies are available for large scale energy storage system, the lead acid technology is considered a low cost option and mature technology that is suitable in rapid charge/discharge large bulk storage system but the low energy density and limited life cycle are considered the main disadvantage of this technology (Ribeiro *et al*., 2001).

Several works have discussed standalone hybrid systems based on renewable energy sources: Energy flow and management of a hybrid WECS/PVECS/fuel cell is performed using wind and PV energies as main energy

Corresponding Author: A. Yasin, Scuola Superiore di Catania, Via Valdisavoia 9, Catania, Italy
Tel: +39 095-2338518 Fax: +39 095-360955

sources while the fuel cell and electrolyser are used as a storage system (El-Shatter *et al*., 2006). Simulation results of dynamic behaviour of a stand-alone hybrid power generation system of WECS, PVECS, micro turbine and BESS are shown (Celik, 2002). The performance of a stand-alone renewable energy system using hydrogen as an energy storage system is evaluated (Agbossou *et al*., 2004). Dynamic modelling of renewable energy sources in the hybrid systems with various control strategies were presented by Candusso *et al*. (2002), Iqbal (2003) and Wang (2006).

This study addresses dynamic modelling and control of a standalone hybrid system based on WECS/PVECS/BESS with time domain stability and performance analysis. WECS and PVECS are used as primary energy sources, while BESS is used as a backup source and storage system. PVECS and WECS are controlled to track the maximum power point (MPPT). BESS is controlled in a manner to stabilize the DC bus voltage by controlling the attached DC/DC bidirectional converter. Time domain performance analysis is presented in this study to check up the control strategies implemented in the system as well as the dynamic system response.

The performance analysis is an important issue in the standalone hybrid systems based on renewable energy sources. The output power of wind turbines is mostly fluctuating and negatively affects the system frequency (Senjyu *et al*., 2005). The PVECS is not an exception as the generated power depends on variable solar radiations. The variation of the load demand is another factor that affects the system stability.

The analysis performed in this study is based on accurate models with controllable power converters. The frequency deviation, DC bus voltage stability and voltage THD are used as indexes for system performance.

PVECS and WECS studied in this paper are based on commercial devices installed in CNR/ITAE of Messina/Italy in hybrid plant using AC bus. This is a preliminary analysis to consider in future the topology of DC bus.

SYSTEM CONFIGURATION

Figure 1 shows schematic diagram of a standalone hybrid system based on WECS, PVECS and BESS, while Fig. 2 shows the Matlab/Simulink/SimPowerSys™ model of the system. In this integrated system, all necessary measurements are performed in order to be fed into the controller which is responsible for providing control signals to all components after evaluation.

When there is an excess in power generation from sun and wind with respect to load requirements, the system charges BESS. In case of insufficient generation BESS covers the deficiency in load demand as it is sized to fill the shortage in most circumstances. If BESS is fully charged, the excess power is transferred to dump load. The system sizing is beyond the purpose of this study. Details about parameters of the three main subsystems of the considered plant are given in Table 1.

Table 1: PVEC, WEG and BESS main data

PVCS	
Module model	Solyndra®-SL001-157
Module unit	157Wp at STC
Module open circuit voltage	92.5 V
Module number	3×4 = 12
Power rating	1.88 kWp
WECS	
Model	TN-1.5 Nozzi Nord
Rated power	1.5 kW
Cut in/cut out speed	4 and 20 m sec^{-1}
Generator type and ratings	1.5 kW PMSG @ 50 Hz
BESS	
Battery (lead acid)	4.6 kWh at 96 V

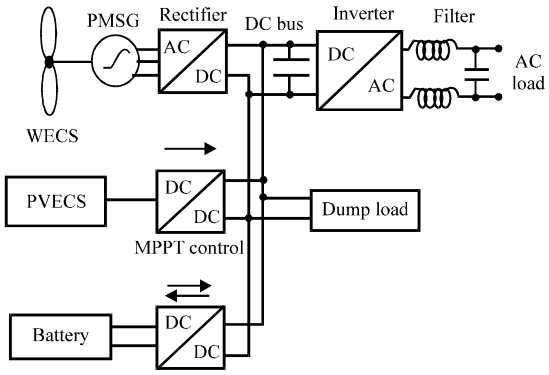

Fig. 1: Schematic diagram of hybrid system based on Wind/PV/BESS

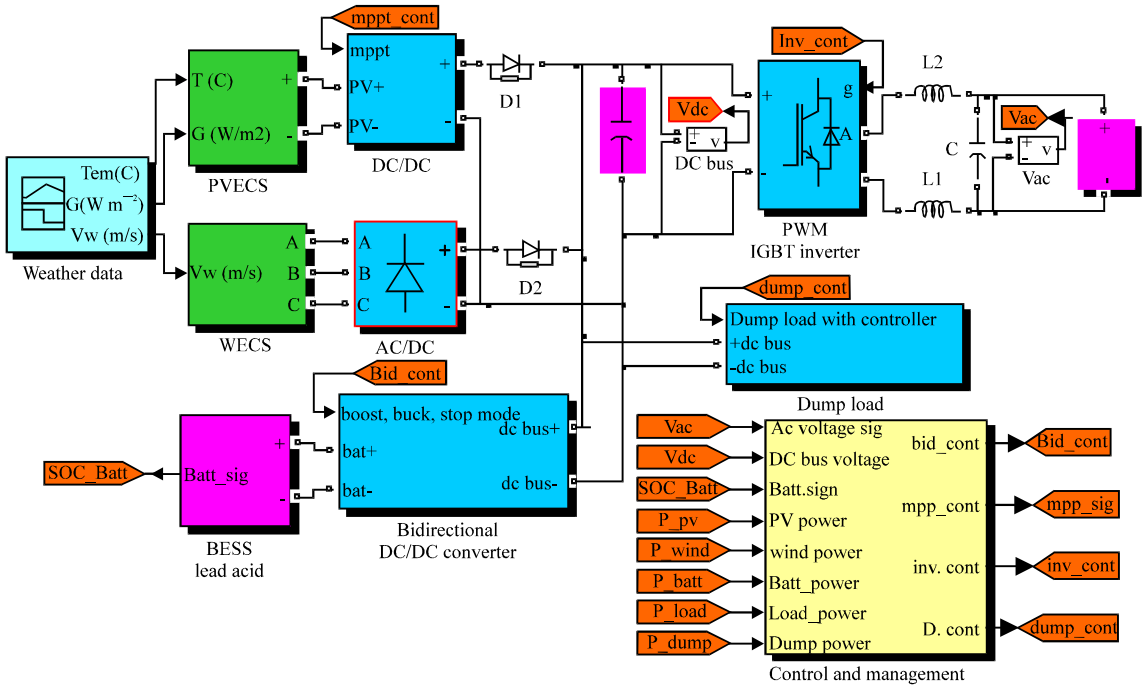

Fig. 2: Simulink model of the WECS/PVECS/BESS hybrid system

MODELLING AND CONTROL OF THE HYBRID SYSTEM COMPONENTS

PVECS is equipped with a step up DC/DC converter controlled by the MPPT algorithm; WECS is controlled for maximum power tracking using the power coefficient curve (Cp) provided by the manufacturer in which a rectifier is attached to convert AC power to DC power. BESS is connected with the DC bus via DC/DC bidirectional converter which is controlled by a specific control strategy. The system supplies the AC load via a single phase inverter.

WECS and PVECS are individually controlled to obtain the maximum power, in which each source provides the DC bus with the corresponding current (I_w and I_{pv}). A diode is attached with each source to make the power flow passes in one direction and to disconnect the energy source in case of fault (Das *et al*., 2005).

Modelling and control of PVECS: A photovoltaic cell converts photon energy directly into electric energy in the form of direct current which means that a photovoltaic device model must be based on the electrical characteristics. PVECS model involves the following parameters:

a : The ideality factor
I : Operation current of the array (A)

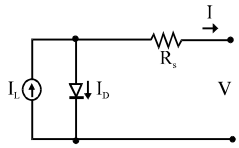

Fig. 3: One-diode photovoltaic cell equivalent circuit model with four parameters

I_L : Light current of array (A)
I_0 : Diode reverse saturation current (A)
k : Boltzmann's constant (J/°K)
K_v : The voltage coefficient temperature, V/C°
k_i : The current coefficient temperature, A/°C
Ns : Number of cells in the panel connected in series
q : Electron's charge
R_s : Equivalent series resistance of the array (Ω)
T : PV cell temperature at STC in Kelvin (°K)
V : Operation voltage of the array (V)
V_t : Thermal voltage of the array (V)

A PV cell model using one-diode equivalent circuit with five parameters is presented by Loferski (1972), In this study, more simplified model is used depending on one-diode with four parameters model as shown in Fig. 3. PVECS is modelled according to the following equations, where the relationship between current and terminal voltage is illustrated (Rauschenbach, 1980; Sera *et al*., 2007; Ross and Smockler, 1986):

$$I=I_L - i_o\left[\exp\left(V+RS\frac{I}{V_t a}\right)-1\right] \quad (1)$$

$$V_t=\frac{N_s kT}{q} \quad (2)$$

$$I - I_o \exp\left(\frac{V_{oc}}{N_s V_t}\right) \quad (3)$$

$$V_{oc}(T) = V_{oc}k_v(T_{cell}+T_{stc}) \quad (4)$$

$$I_{sc}(T)=\left(1+\frac{k_i}{100}(T_{cell}-T_{stc})\right) \quad (5)$$

The value of cell temperature can be derived using empirical (Eq. 6) which depends on Nominal Operating Conditions Temperature (NOCT), NOCT is the temperature of the cell at 800 W/m^2 irradiance and 20°C of ambient temperature (Ross and Smockler, 1986):

$$T_{cell}=T_{ambient}-\frac{NOCT}{0}.8G \quad (6)$$

Solyndra® solar array of capacity 1.88 kWp depending on amorphous silicon (a-Si) technology is used and modelled in this study. Each module (SL001-157) is of 157 Wp at 92.5 V open voltage (Alwitra, 2010). The installed system consists of 3 strings connected in parallel in which each string consists of 4 modules connected in series.

The I-V and P-V characteristics of the used photovoltaic module operating at different solar radiation and at constant temperature of 25°C are shown in Fig. 4. It can be shown from the characteristics that PV power is greatly dependent on solar radiation in which the maximum power obtained from the PVECS module is 156 W at standards conditions which is consequence with the manufacturer's data sheet; this is considered a validation for the PV model used in this study.

Due to high cost of photovoltaic cells, PVECS must be controlled to obtain MPP all the time, several MPPT techniques are used as perturbation and observation method (P and O), incremental conductance method and current or voltage-based MPPT (Masoum *et al*., 2002).

Perturbation and Observation (P and O) method is used in this study. This method is widely used because of its simplicity structure and the few measured parameters. The working principle of these algorithms are summarised as following: The array terminal voltage is periodically perturbing (increase or decrease) and another algorithm for comparing the PV output power with the previous perturbation cycle. The perturbation will go to the same direction in case of the positive power difference while reversing the direction in case of negative power difference (Hussein *et al*., 1995).

The DC/DC converter is considered a main component in this method that is acting as an interface between PV system array and DC bus. The converter topology used in this study with control scheme is shown in Fig. 5.

Figure 6 shows the performance and the validity of P and O MPPT control scheme used in this study by showing up the power generated from the same PVECS system with/without MPPT control scheme.

Modelling and control of WECS: TN-1.5 Nozzi Nord wind turbine of capacity 1.5 kW (micro) has been modelled. It has been devised to fit onto the roofs of buildings. Due to its vertical axis format with three helical blades the micro turbine is able to harness wind power from every direction achieving more consistent power generation and a low level of acoustic emissions.

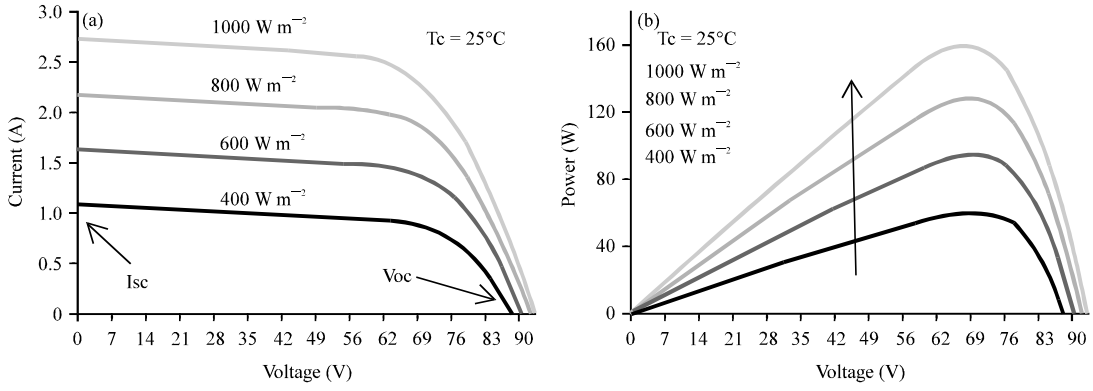

Fig. 4(a-b): I-V and P-V characteristics of the used photovoltaic module

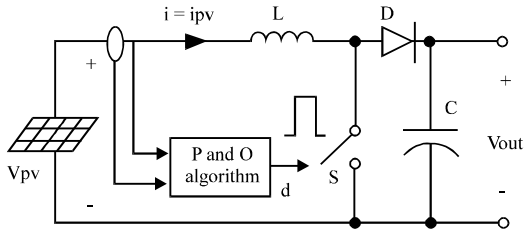

Fig. 5: DC/DC boost converter topology controlled by MPPT control scheme

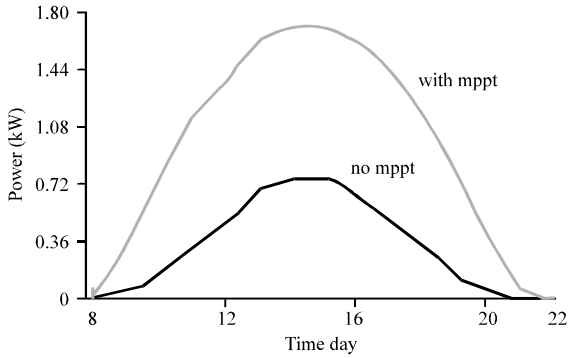

Fig. 6: PV system with/without MPPT control

Wind turbine is fitted with Permanent Magnet Synchronous Generator (PMSG) built especially for this type of application (http:// www. tozzinord.com/admin/ PagPar.php?op=fg& id_pag_par= 188&fld=file).

The mathematical model of WECS system depends on the following equations which are based on the following parameters:

A_t : Swept area of the turbine (m^2)
C_p : Wind power coefficient
F : Combined viscous friction of rotor and load ($N.m.s.rad^{-1}$)
i_q, i_d : q and d axis currents (A)
J : Combined inertia of rotor and load (kg. m^2)
L_q, L_d : q and d axis inductances (H)
p : Number of pole pairs
P_t : Wind turbine power (W)
R : Resistance of the stator windings (Ω)
T_e : Electromagnetic torque (N.m)
T_t : Shaft mechanical torque (N.m)
V_w : Wind velocity (m/s)
V_q, V_d : Q and d axis voltages (V)
ρ_a : Air density (kg m^{-3})
ω_r : Angular velocity $d\theta/dt$ ($rad.s^{-1}$)
θ : Rotor angular position (rad)
λ : The amplitude of the flux induced by the permanent magnets of the rotor (Wb)
Ω : Rotational speed of the blade (rpm)

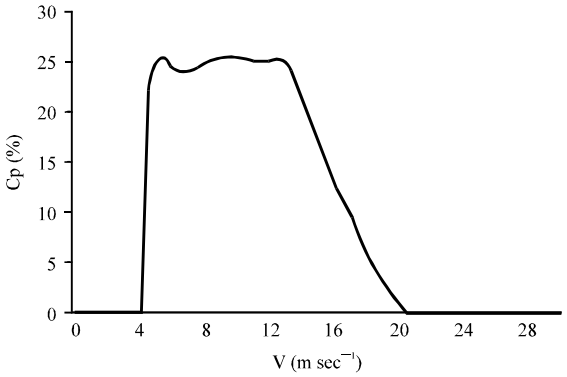

Fig. 7: Power coefficient versus different wind speeds

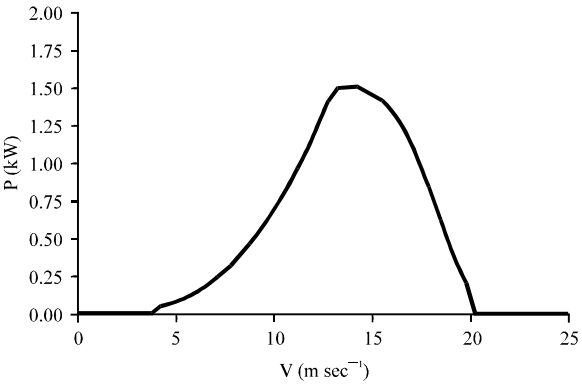

Fig. 8: Wind turbine output power characteristic

The power generated from the rotor turbine wind is given by Eq. 7 (Muljadi *et al*., 1996; Manwell *et al*., 2003):

$$P_t \frac{1}{2} \rho a C_p A_t v_w^3 \quad (7)$$

The curve that illustrates relationship between power coefficient (Cp) and wind speed is shown in Fig. 7 (http://www.tozzinord.com/admin/PagPar. php? op=fg& id_pag_par=188 and fld=file). This coefficient is defined as the aerodynamic efficiency of the wind turbine as a function of tip speed ratio. The Tip Speed Ratio (TSR) is defined as the ratio between the peripheral speed of the blades and the wind speed. This curve facilitates the calculation of the maximum power that can be extracted from wind turbine at various wind speeds.

Figure 8 shows the manufacturer wind turbine output power characteristics of the WECS used in this study at different wind velocities. It can be observed that the output power is kept constant at higher wind velocities even though the wind turbine has the potential to produce more power. This is done to protect the electrical system and to prevent the over speeding of the rotor. The

main characteristics of the wind turbine like cut-in, cut-off, nominal wind speed which are 4, 20 and 13 m sec^{-1}, respectively are also shown in Fig. 8.

The wind turbine torque on the shaft can be calculated from the wind power as in Eq. 8, in which the rotational speed of the blades (Ω) is measured from the mechanical model of the PMSG:

$$T_t = \frac{P_t}{\Omega} = \frac{1}{2}\rho a C_p A_t \frac{V_w^3}{\Omega} \quad (8)$$

The generated torque (T_t) is used as an input mechanical power to electrical generator. The mechanical system of the electrical generator is represented by Eq. 9 (Krause *et al*., 2002):

$$\frac{d}{dt}w_r = \frac{1}{J}(T_e - Fw_r - T_t) \quad (9)$$

In this study, the built in SimPowerSys™ block model of a permanent magnet synchronous machine is used as a power generator driven by the wind turbine, the sinusoidal electrical model in the synchronous reference frame (dq) is given in Eq. 10-12) (http://www.mathworks.com/help/toolbox/physmod/powersys/ref/permanentmagnetsynchronousmachine.html?):

$$\frac{d}{dt}i_d = \frac{1}{L_d}v_d - \frac{R}{L_d}i_d + \frac{L_q}{L_d}pw_r i_q \quad (10)$$

$$\frac{d}{dt}i_q = \frac{1}{L_q}v_q - \frac{R}{L_q}i_q + \frac{L_q}{L_q}pw_r i_d - \frac{\lambda pw_r}{L_q} \quad (11)$$

$$T_e = 1.5\ p\ [\lambda i_q + (L_d - L_q) i_d i_q] \quad (12)$$

Figure 9 shows the schematic diagram of the WECS model. Figure 10 illustrates simulation results that have been carried out to verify and validate the proposed WECS model, the response of the WECS model at variable wind speed is shown below.

Modelling and control of BESS and DC bus: The capacity of BESS consists of 4.6 kWh of lead acid type at terminal voltage of 96 V. The commercial name is 'EnerSys-G16EPX (16 Ah)'. BESS consists of 3 strings connected in parallel in which each string consists of 8 batteries connected in series to form 96 V and 4.6 kWh. The parameters used in the model are illustrated as following:

A : The exponential zone amplitude (V)
B : The exponential zone time constant inverse (Ah^{-1})
E_{batt} : No load voltage (V)
E_0 : Battery constant voltage (V)
I_{batt} : Battery charging and discharging current (A)
K : Polarisation voltage (V)
Q : Battery capacity (Ah)
R_{in} : Internal resistance of the battery (Ω)
V_{batt} : Terminal voltage of the battery (V)

The built-in SimPowerSys™ block model of lead acid battery is used in this study where it is modelled by a constant resistance connected in series with a controlled voltage source as shown in Fig. 11 (http://www.mathworks.com/help/toolbox/physmod/powersys/ref/battery.html?), a constant resistance is assumed during the different modes of battery. The controlled source is described in the following equations (Tremblay *et al*., 2007):

$$E_{batt} = E_0 - K\frac{Q}{Q - it} + Ae^{-B.it} \quad (13)$$

$$V_{batt} = E_{batt} - R_{in}.I_{batt} \quad (14)$$

The DC bus voltage (V_{DC}) is designed to be within the constant range (380-420 V). Root mean square value of the inverted voltage (V_{rms}) after being filtered is fixed to 230 V at 50 Hz. The value of the DC bus voltage is

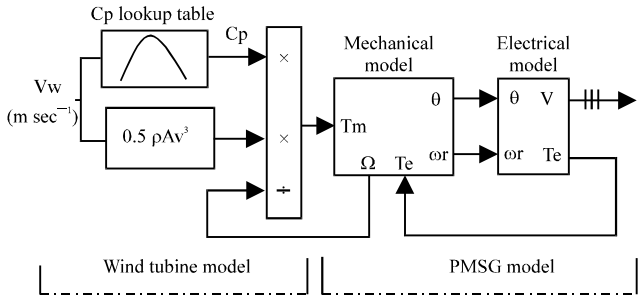

Fig. 9: Schematic diagram of WECS model

sensitive to load and weather conditions. It includes a capacitor with high capacitance that collects energy from different sources.

In order to extend the life time of the battery, it is good practice not to overcharge/over discharge it. This could be achieved by keeping the state of charge (SOC) within the safe range. DC bus is controlled in order not to exceed the maximum specified value (V_{max} = 420 V) and not to exceed the minimum specified value (V_{min} = 380 V). This also protects BESS against frequent variation in the operation modes.

DC/DC bidirectional converter works in a buck mode to charge the battery with excess power and in a boost mode to discharge it to fill up the gap of power deficiency. Stop mode is called whenever BESS is overcharged or has no sufficient charge to deliver.

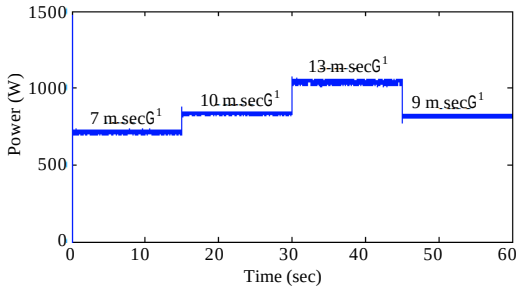

Fig. 10: Output power of the WECS model at different wind speeds

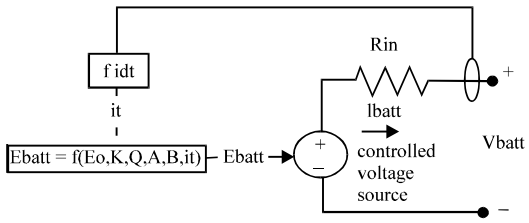

Fig. 11: Equivalent electrical circuit of the lead battery

In the proposed control strategy, BESS plays a major role in regulating DC bus voltage through a DC/DC bidirectional converter. This indirectly manages the energy exchanges between power generation and the storage system.

Control of the DC/DC bidirectional converter is achieved using a Fuzzy Logic Controller (FLC). The main requirement of control algorithm is to determine the working mode of the bidirectional converter. The main function of the FLC is to make a relation between the output values to inputs using rules built with 'IF...THEN' statements. This type of control is very suitable when it is difficult to determine whether the input is a member of a given set (logic 1) or not (logic 0) as in Boolean logic. FLC deals with the cases that change anywhere in the range of 0-1 (Bose, 2000). This means that FLC provide more practical output signal instead of 0 or 1 logic output signal.

FLC model is constructed using mamdani inference with two input variables and one output as shown in Fig. 12. DC bus voltage and battery SOC are the input variables and the operation mode of bidirectional converter is the output variable. Three linguistic terms for membership functions for the DC bus voltage are 'minimum', 'normal' and 'maximum'. BESS SOC has three membership functions that are 'empty', 'medium' and 'full'. Using the data available from these two inputs, FLC determines the operation mode which corresponds to the output of the model which has three membership functions that are 'buck', 'boost' and 'stop' mode.

FLC utilizes the two inputs and generates the operation mode of the converter as shown in Fig. 13.

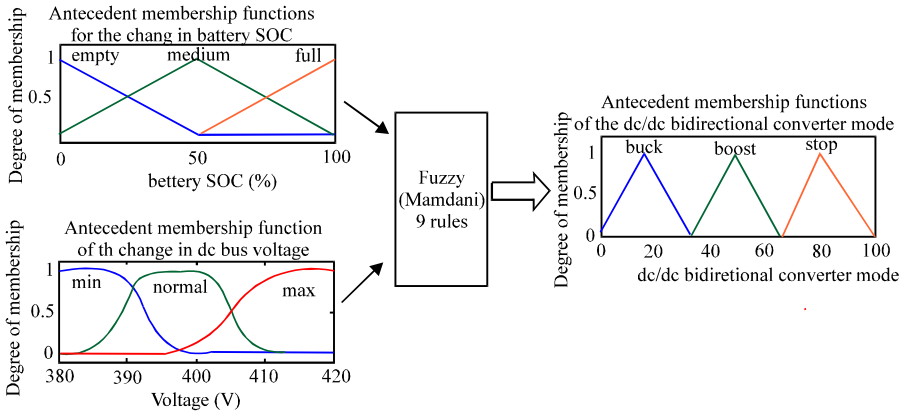

Fig. 12: Fuzzy inference system

The DC/DC (buck-boost) bidirectional converter consists of two main switches (S_1, S_2) with inductor as shown in Fig. 14. S_1 and S_2, once activated, are responsible for maintaining the buck mode and boost mode, respectively. Another switch (S_3) is installed for stop mode. The control scheme is depicted in Fig. 15. DC bus voltage ($V_{DC\text{-}bus}$) is sensed and compared with the reference voltage (V_{ref}). The error will be regulated by the PI voltage controller to generate BESS reference current (I_{bat_ref}) which will be compared with the actual battery current, the error will be regulated by the PI current controller. The control signals of buck switch (S_1) and boost switch (S_2) are both generated, where the control law of the boost signal is the complement of the buck signal. The control signal sent by FLC determines the working mode of the DC/DC bidirectional converter. The values of PI parameters are shown in Table 2.

Table 2: Controllers parameters

	DC/DC bidirectional converter		
	Voltage controller	Current controller	Inverter
Kp	0.5	1	20
Ki	10	500	2
Kd	0	0	1

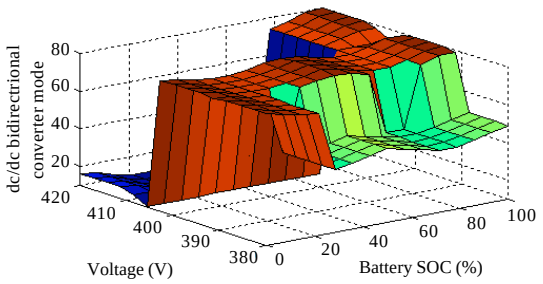

Fig. 13: FLC surface for bidirectional DC/DC converter mode

Modelling and control of the DC/AC inverter: DC bus collects the energy generated by the renewable energy sources and supplies it through a single phase inverter. The inverter is controlled using the PWM technique to ensure voltage sine wave signal at the load side with the required amplitude and frequency after being filtered by low pass filter. Figure 16 shows the single phase full bridge inverter topology used in this study. This inverter converts the DC bus voltage to a regulated AC voltage with the required amplitude and frequency by switching the bridge in appropriate sequence.

The switching sequence of the inverter is varied depending on the feedback signal sensed from the load side voltage, where it is compared with a reference sinusoidal signal of a standard frequency and amplitude. The error enters a PID controller which provides the unipolar PWM generator with a reference control signal. The suitable controller parameters are shown in Table 2. The low pass filter attached to the inverter is designed to ensure the ripple free power for the electrical appliances; the designed values of inductances are 1 mH for each and 75 μF for the capacitor.

The dump load consists of a power converter and a bank of resistors. The nominal power of dump load is chosen to be a 30% greater than nominal power extracted from PVECS and WECS, so that the isolated power system can be controlled even in the case of no load and BESS is fully charged or failed (Sebastia and Quesada, 2006).

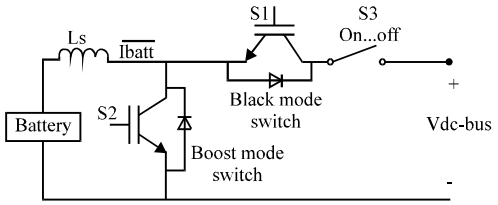

Fig. 14: Bidirectional DC/DC converter

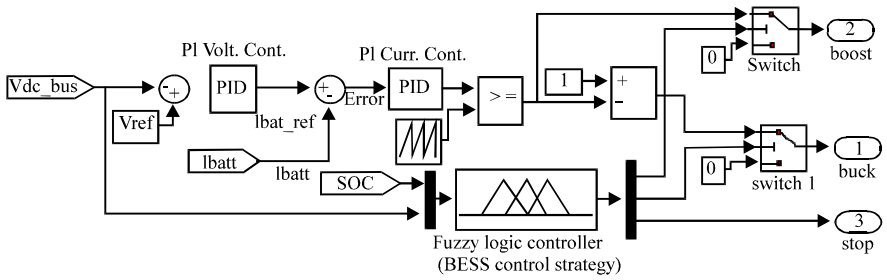

Fig. 15: Control scheme of the DC/DC bidirectional converter

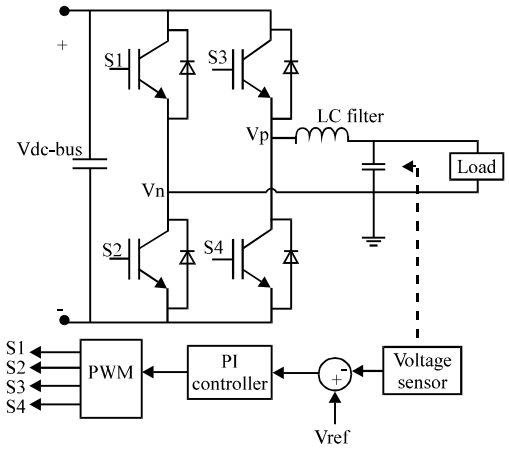

Fig. 16: Single phase DC/AC full bridge topology with control scheme

TIME DOMAIN ANALYSIS

This section illustrates different cases that may be occurred during the operation of the stand-alone hybrid system. Three cases are considered on the basis that weather data and load demand are instantaneously varied during the day. In order to study the behaviour of the system under same conditions, same load profile is applied in all cases. The ambient temperature is assumed to be constant (25°C) throughout the simulations.

The dynamic behaviour of the hybrid system for each case is analyzed, per unit system is used to express the power flow through the system. The solar radiation is expressed in per unit system in which 1000 W m^{-2} equals to 1 in per unit system, the wind speed is expressed in the actual values.

The frequency deviation, stability of DC bus voltage and voltage total harmonic distribution (THD_V) are taken as system performance indexes.

Frequency deviation is considered an important index and the normalized frequency deviation is calculated as shown in Eq. 15:

$$\Delta f = \frac{f - fr}{fr} \quad (15)$$

where, fr is the rated frequency (50 Hz) and f is the measured frequency (Hz). According to standard EN50160/2006, under normal operating conditions, the mean value of the fundamental frequency of islanding system (standalone) measured over 10 sec must stay within range: 50 Hz±2% (Baggini, 2008). Δf is adopted in this study as a stability index, which allowing evaluation of a small frequency variation.

The Simulink model shown in Fig. 17 illustrates the method of measuring Δf in the model. Once the voltage signal is sensed, each voltage cycle is transferred to a pulse in the output of the flip flop. The two switches and clock are used to count up the time between the two successive pulses. The measured frequency (1/T) is compared and divided with the rated frequency (fr) to calculate the frequency deviation as illustrated in Eq. 15.

Variation in DC bus voltage is taken as a system stability index. In general, the variation of voltage is caused from sudden changes in load and weather conditions. DC bus voltage is controlled to be within the range (380-420 V). The DC bus voltage is normalized at 400 V base value.

THD_V is an important index to evaluate the quality of output AC signal and it is taken into account in this analysis. It is calculated using the following equation:

$$THD_v = \sqrt{\sum_2^{\infty} V_h^2} \Big/ V_1 \quad (16)$$

The power flow in the system in all circumstances is governed by this general relation:

$$P_{net} = P_{WECS} + P_{PVECS} - P_{load} \quad (17)$$

where, P_{net} is the net generated power, P_{PVECS} and P_{WECS} are, respectively the power generated from PVECS and WECS. P_{load} is the load power.

If $P_{net}>0$, there is an excess of generated power while if $P_{net}<0$, the generated power is insufficient. The excess power is supplied to BESS. However, if the excess power is greater than the BESS rated power, part of the energy is transmitted to the dump load. If a lack of power is detected the BESS compensates the deficiency.

Case 1: WECS/BESS: In this case the WECS is connected to the system to generate power (P_{WECS}) while PVECS is disconnected (P_{PVECS} = 0) as shown in Fig. 18, this condition may happen during the night when the solar radiation is zero. Results of time domain simulation of case 1 is shown in Fig. 19 where each period is analysed as following:

Period (0-30 sec): The average wind speed in this period is 7.5 m sec^{-1} and the average load is 1 pu which represents the base behaviour of the system to high extent. WECS generates about 0.5 pu, whereas BESS fills the deficiency in the generated power which is about 0.5 pu. The DC bus voltage is within the allowable lower range.

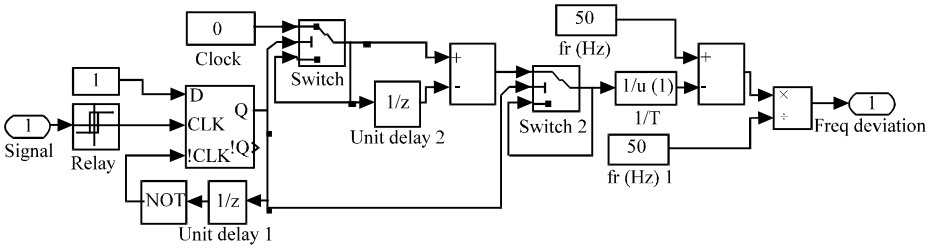

Fig. 17: Simulink model for frequency deviation measurement

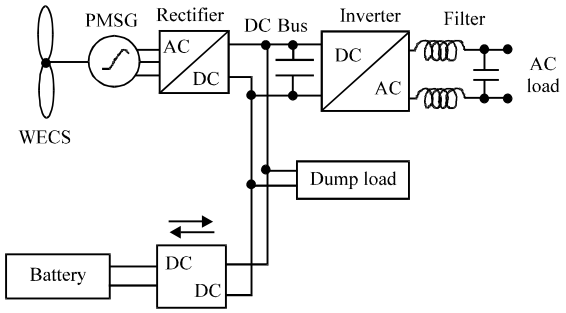

Fig. 18: Schematic diagram of the hybrid system in Case 1 (WECS/BESS)

Period (30-60 sec): A big and sudden rise in load demand (2.23 pu) occurs and the wind speed rises to 9 m sec^{-1} to increase the extracted power to about 0.8 pu. BESS provides system with about 1.4 pu which is the deficiency in the generated power from the WECS to cover the load. The DC bus voltage is decreased to the lowest allowable value (0.95 pu).

Period (60-90 sec): A sudden drop occurs in the load (0.5 pu) and in wind speed (7.5 m sec^{-1}). This period resembles the first period in all features which proves that sudden falling down in load demand and wind speed never affect the system stability. A small dip has been occurred in DC bus voltage (0.975 pu).

Period (90-120 sec): A sudden rise in the load (1 pu) and in wind speed (11 m sec^{-1}). The power generated is less than the load demand. BESS cover the small deficiency.

Period (120-150 sec): A sudden drop in the load demand (0.5 pu) and wind speed (7.5 m sec^{-1}) are occurred. Power generated is less than the load demand, which makes BESS cover the small deficiency.

Case 2: PVECS/BESS: In this case PVECS is connected to the system while WECS is disconnected as shown in

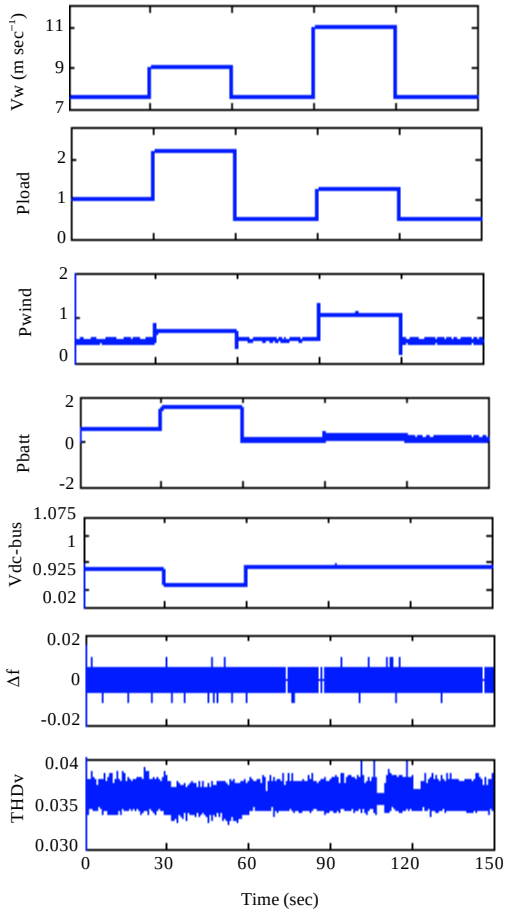

Fig. 19: Time domain simulation of Case 1

Fig. 20. Results of time domain simulation of case 2 is shown in Fig. 21 where each period is analysed as following:

Period (0-30 sec): The average solar radiation is gradually rises from 0.35 to 0.5 pu while load demand is 1 pu. The generated power doesn't cover the load demand which

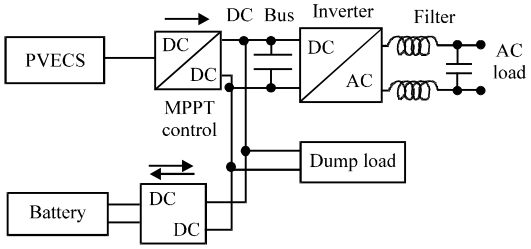

Fig. 20: Schematic diagram of the hybrid system in Case 2 (PVECS/BESS)

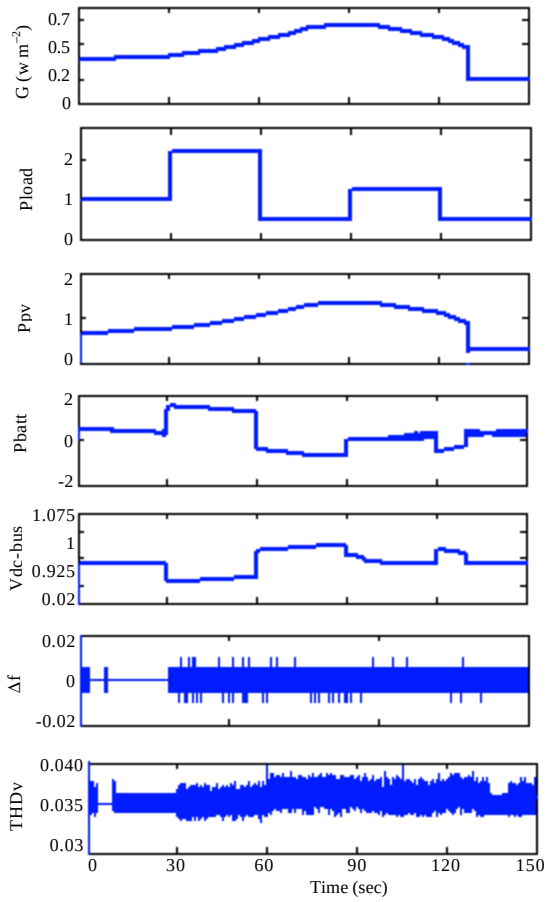

Fig. 21: Time domain simulation of Case 2

makes BESS working in discharging mode. The power provided from BESS is gradually decreasing with the gradual increase in solar radiation. DC bus voltage is less than 1 pu but still within the accepted range.

Period (30-60 sec): A sudden rise in the load demand (2.23 pu) and the solar radiation increases with constant rate. BESS responds immediately to cover the deficiency in generated power. Δf increases with respect to the previous period but still within the range with some sparks as shown in the Fig. 20. DC bus voltage drops to the lowest accepted value.

Period (60-90 sec): A sudden drop in load (0.5 pu) with gradual increase in solar radiation (0.6 pu). The generated power exceeds the load demand which drives BESS to charging mode. The charging power increases with the rise in solar radiation. Δf is still within in the accepted range with little sparks. THD_V increases with respect to previous periods. DC bus voltage keeps stable but with the upper control range (1.025 pu).

Period (90-120 sec): A sudden rise in load demand (1 pu) with decreasing rate in solar radiation (0.6 pu). The power generated is less than load demand which switches gradually BESS to discharging mode.

Period (120-150 sec): A sudden drop in load demand (0.5 pu) and gradual drop occurs in solar radiation until the 130 sec. BESS is charged by the generated surplus power and the DC voltage increases. After this time a sudden drop occurs (0.35 pu) which drives BESS to discharging mode.

Case 3: WECS/PVECS/BESS: In this case PVECS and WECS are connected as shown in Fig. 1. Results of time domain simulation of case 3 is shown in Fig. 22 where each period is analysed as following:

Period (0-30 sec): The average solar radiation increases gradually from 0.35 to 0.5 pu while the average wind speed and load is 7.5 m sec^{-1} and 1 pu, respectively. The generated power covers the load demand which makes BESS working in the charging mode.

Period (30-60 sec): A sudden increase in the load demand (2.23 pu) and the wind speed increases to 9 m sec^{-1}, while the solar radiation increases with constant rate. BESS works in discharging mode to cover the big deficiency in power. Δf is still within accepted range with some sparks. DC voltage keeps within the range (0.975-1.025 pu).

Period (60-90 sec): A sudden drop in load (0.5 pu) and in wind speed (7.5 m sec^{-1}) with gradual increase in solar radiation (0.6 pu). The generated power exceeds the load demand which drives BESS to charging mode (1 pu). Δf is still within in the range with little sparks. DC voltage keeps stable but with the upper control range (1.025 pu).

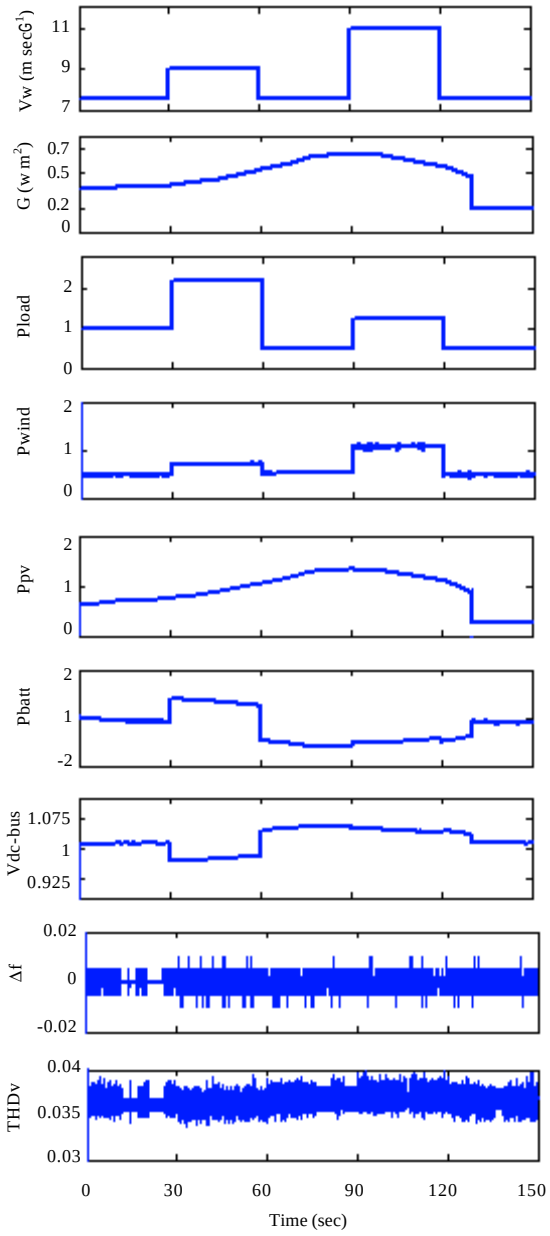

Fig. 22: Time domain simulation of Case 3

Period (90-120 sec): A sudden rise in load demand (1 pu) and in wind speed (11 m sec^{-1}) with constant solar radiation (0.6 pu). The power generated exceeds the load demand which keeps BESS in the charging mode (0.8 pu). Δf is within the range and DC voltage is stable at the upper range.

Period (120-150 sec): A sudden drop in the load demand (0.5 pu), wind speed (7.5 m sec^{-1}) and in the solar radiation (0.35 pu). The power generated is still exceeding the load demand which makes BESS working in the charging mode.

From previous analysis, it is clear that the system is maintained stable in all cases and intervals even at different weather conditions and sudden changes in load demand as it is possible to observe from the Δf diagram. In fact, the normalized frequency deviation is always less than 0.02; moreover, the DC bus voltage remains constant around 1 pu. THD_V doesn't exceed 0.05 all over the five intervals of the three cases which is within standard design requirements (IEEE Standards 519-1992, 1993).

The degree of stability is different in each case, for example, in case 1 DC bus voltage is within the lower range and at case 3 it is mostly within the highest range. The transient change in load demand affects the stability of DC bus voltage, especially in cases 1 and 2.

In case 1 and 2, BESS mostly works in discharging mode to cover the deficiency in load demand while in case 3 it mostly works in charging mode. Δf is within the range in all cases but in case 3 greater number of sparks are noticed, this is may be due to the availability of two power sources (PVEC and WECS) in the system. THD_V is less than 0.04 in all cases; this is a good indication for the good performance of AC output signal under different weather conditions and load demand.

CONCLUSION

This study has proposed a standalone hybrid system based on WECS, PVECS and BESS in order to electrify a residential house even with the intermittent power output nature of WECS and PVECS. The system is accurately modelled using MatLab/Simulink/SimPowerSys™ depending on manufacturer's parameters of each component. The system is locally controlled to extract the MPP from WECS and PVECS and globally controlled to ensure system performance and suitable power flow between different renewable energy sources and BESS. A control method has been proposed to control the DC bus voltage and the energy flow between different energy sources.

Time-domain performance analysis has been performed under three different cases. Each case includes base states, sudden rise and sudden drop of wind speed, solar radiation and load demand. To put the system under same situation, the load demand is the same for all cases. Each dynamic response of the practical wind speed, solar

radiation and load demand is analyzed and discussed in terms of normalized frequency deviation, DC bus voltage stability and THD_V of the output signal. Results of simulations ensure the effectiveness of the proposed system to follow up the variations in the load demand under weather data described in the different cases.

REFERENCES

Ackermann, T., 2005. Wind Power in Power System. John Wiley and Sons, UK.

Agbossou, K., M. Kolhe, J. Hamelin and T.K. Bose, 2004. Performance of a stand-alone renewable energy system based on energy storage as hydrogen. IEEE Trans. Energy Conversion, 19: 633-640.

Alwitra, 2010. Brochure solyndra. Alwitra Company. http://www.alwitra.de/index.php?id=produkte&L=1&tx_abdownloads_pi1%5baction%5d=getviewclickeddownload&tx_abdownloads_pi1%5buid%5d=93 and cHash=dc818c6e85.

Baggini, A., 2008. Handbook of Power Quality. John Wiley and Sons Ltd., The Atrium, Southern Gate, Chichester, West Sussex PO19 8SQ, England, ISBN-10:0470754230, Pages: 642.

Bose, BK., 2000. Fuzzy logic and neural networks in power electronics and drives. IEEE Ind. Applied Mag., 6: 57-63.

Candusso, D., L. Valero and A. Walter, 2002. Modelling, control and simulation of a fuel cell based power supply system with energy management. Proc. 28th Annu. Conf. IEEE Ind. Electron. Soc., 2: 1294-1299.

Celik, A.N., 2002. The system performance of autonomous photovoltaic-wind hybrid energy systems using synthetically generated weather data. Renewable Energy, 27: 107-121.

Das, D., R. Esmaili, L. Xu and D. Nichols, 2005. An optimal design of a grid connected hybrid wind/photovoltaic/fuel cell system for distributed energy production. Proceedings of the 31st Annual Conference of IEEE Industrial Electronics Society, November 6-10, 2005, Raleigh, North Carolina, pp: 2499-2504.

El-Khattam, W. and M.M.A. Salama, 2004. Distributed generation technologies, definitions and benefits. Electric Power Syst. Res., 71: 119-128.

El-Shatter, T.F., M.N. Eskander and M.T. El-Hagry, 2006. Energy flow and management of a hybrid wind/PV/fuel cell generation system. Energy Conversion Manage., 47: 1264-1280.

Grandi, G., D. Casadei and C. Rossi, 2003. Direct coupling of power active filters with photovoltaic generation systems with improved MPPT capability. Proceedings of the IEEE Bologna Power Tech Conference, June 23-26, 2003, Italy, pp: 1-6.

Hussein, K.H., I. Muta, T. Hoshino and M. Osakada, 1995. Maximum photovoltaic power tracking: an algorithm for rapidly changing atmospheric conditions. Proc. IEE Generat. Transm. Distribut., 142: 59-64.

IEEE Standards 519-1992, 1993. IEEE recommended practices and requirements for harmonic control in electric power systems. IEEE Industry Applications Society, http://ieeexplore.ieee.org/servlet/opac?punumber=2227.

Iqbal, M.T., 2003. Modelling and control of a wind fuel cell hybrid energy system. Renewable Energy, 28: 223-237.

Krause, P.C., O. Wasynczuk and S.D. Sudhoff, 2002. Analysis of Electric Machinery and Drive Systems. 2nd Edn., John Wiley and Sons, New York, New York, ISBN: 978-0-471-14326-0, pp: 632.

Kuo, Y.C., T.J. Liang and J.F. Chen, 2001. Novel maximum-power-point-tracking controller for photovoltaic energy conversion system. IEEE Trans. Ind. Electron., 48: 594-601.

Loferski, J.J., 1972. An Introduction to the Physics of Solar Cells. In: Solar Cells: Outlook for Improved Efficiency, NRC and Ad Hoc Panel on Solar Cell Efficiency (Eds.). National Academy of Sciences, Washington, DC, pp: 47-53.

Manwell J.F., J.G. McGowan and A.L. Rogers, 2003. Wind Energy Explained. John Wiley and Sons, Ltd., New York.

Masoum, M.A.S., H. Dehbonei and E.F. Fuchs, 2002. Theoretical and experimental analyses of photovoltaic systems with voltageand current-based maximum power-point tracking. IEEE Trans. Energy Conversion, 17: 514-522.

McDowall, J., 2000. Conventional battery technologies-present and future. IEEE Power Eng. Soc. Summer Meet., 3: 1538-1540.

Muljadi E., S. Drouilhet, R. Holz and V. Gevorgian, 1996. Analysis of permanent magnet generator for wind power battery charging. Proceedings of the IEEE Industry Applications Conference, October 6-10, 1996, San Diego, CA, USA., pp: 541-548.

Rauschenbach, H.S., 1980. Solar Cell Array Design Handbook. Van Nostrand Reinhold Company, New York, ISBN: 978-0442268428.

Ribeiro P.F., B.K. Johnson, M.L. Crow, A. Arsoy and Y. Liu, 2001. Energy storage systems for advanced power applications. Proc. IEEE, 89: 1744-1756.

Ross, R.G. and M.I. Smockler, 1986. Flat-plate solar array project final report, Volume 6: Engineering-sciences and reliability. Jet Propulsion Laboratory Publication, National Photovoltaics Program (U.S.), 86-31.

Sebastia R. and J. Quesada, 2006. Distributed control system for frequency control in a isolated wind system. Renew. Energy, 31: 285-305.

Senjyu, T., T. Nakaji, K. Uezato and T. Funabashi, 2005. A hybrid power system using alternative energy facilities in isolated island. IEEE Trans. Energy Convers., 20: 406-414.

Sera, D., R. Teodorescu and P. Rodriguez, 2007. PV panel model based on datasheet values. Proceedings of the IEEE International Symposium on Industrial Electronics, June 4-7, 2007, Vigo, Spain, pp: 2392-2396.

Shimizu T., M. Hirakata, T. Kamezawa and H. Watanabe, 2007. Generation control circuit for photovoltaic modules. IEEE Trans. Power Electron., 16: 293-300.

Tremblay, O., L.A. Dessaint and A.I. Dekkiche, 2007. A generic battery model for the dynamic simulation of hybrid electric vehicles. Proceedings of the IEEE Vehicle Power and Propulsion Conference, September 9-12, 2007, Arlington, TX, pp: 284-289.

Wang, C., 2006. Modelling and control of hybrid wind/photovoltaic/fuel cell distributed generation systems. Ph.D. Thesis, Montana State University, Bozeman, USA.